Optimized aperiodic highly directional narrowband infrared emitters

Christopher H. Granier,[1,*] Francis O. Afzal,[2,3] Changjun Min,[2,4] Jonathan P. Dowling,[1,5] and Georgios Veronis[2,6]

[1]*Hearne Institute of Theoretical Physics and Department of Physics and Astronomy, Louisiana State University, Baton Rouge, Louisiana 70803, USA*
[2]*Center for Computation and Technology, Louisiana State University, Baton Rouge, Louisiana 70803, USA*
[3]*Department of Physics, Truman State University, Kirksville, Missouri 63501, USA*
[4]*Current address: Institute of Modern Optics, Nankai University, Tiajin 300071, China*
[5]*Computational Sciences Research Center, 1000 84 Beijing, China*
[6]*School of Electrical Engineering and Computer Science, Louisiana State University, Baton Rouge, Louisiana 70803, USA*
**Corresponding author: cgrani1@lsu.edu*

Received January 16, 2014; revised March 10, 2014; accepted April 3, 2014;
posted April 15, 2014 (Doc. ID 204523); published May 14, 2014

In this paper, we present optimized aperiodic structures for use as narrowband, highly directional thermal infrared emitters for both TE and TM polarizations. These aperiodic multilayer structures designed with alternating layers of silicon and silica on top of a semi-infinite tungsten substrate exhibit extremely high emittance peaked around the wavelength at which the structures are optimized. Structures were designed by a genetic optimization algorithm coupled to a transfer matrix code that computed thermal emittance. First, we investigate the properties of the genetic-algorithm-optimized aperiodic structures and compare them to a previously proposed resonant cavity design. Second, we investigate a structure optimized to operate at the Wien wavelength corresponding to a near-maximum operating temperature for the materials used in the aperiodic structure. Finally, we present a structure that exhibits narrowband and highly directional emittance for both TE and TM polarizations at the frequency of one of the molecular resonances of carbon monoxide (CO); hence, the design is suitable for the emitting portion of a detector of CO via absorption spectroscopy.

OCIS codes: (350.4238) Nanophotonics and photonic crystals; (260.0260) Physical optics.
http://dx.doi.org/10.1364/JOSAB.31.001316

1. INTRODUCTION

The thermal emittance of both bulk materials and textured structures has been widely investigated in recent years. Bulk thermal emittance sources (such as tungsten) possess incoherent, isotropic, and broadband radiation spectra that vary from material to material; however, it is well known that these radiation spectra can be drastically altered by utilizing textured surfaces [1], multilayer structures, or even three-dimensional constructions [2] possibly in tandem with a bulk material substrate. From highly directional emitters (antennae) to quasi-coherent radiation sources [3,4] (lasers), as well as solar photovoltaics [5,6], these emitters may have many uses due to their emittance spectra altering properties.

Several approaches have been used to achieve narrowband, highly directional thermal emittance. One of these approaches, with one-dimensional photonic crystals, employed a periodic quarter-wave stack with a half-wavelength resonant cavity as well as tungsten or silver substrate. This design resulted in the bulk substrate exhibiting directional, tunable, wavelength-selective emittance [7]. A similar outcome was realized using periodic one-dimensional metallic photonic crystal slabs [8]. Another approach to achieve coherent thermal emittance is to use gratings [9–11] or textured metal surfaces [12]. Other approaches include utilizing metamaterials [13] or shock waves propagating through a crystal [14,15] to achieve this end. Finally, narrowband, highly directional transmittance can be achieved by a photonic heterostructure consisting of two one-dimensional defective photonic crystals [16].

In this paper, we focus on aperiodic multilayer structures of alternating layers composed of silicon and silica above a tungsten substrate to produce narrowband, highly directional thermal emission for both TE and TM polarizations. One-dimensional layered structures without texturing are preferable to more complex two- and three-dimensional structures because of the relative ease and low cost of fabrication. Our narrowband, highly tunable infrared emitter exhibits highly narrow angular emittance. We achieve this emittance profile by utilizing a genetic optimization algorithm [17] to select each layer's thickness independently so that the structure is completely aperiodic. The choice of the fitness function proved crucial in obtaining structures with narrowband highly directional emittance. Such a device should have applications not only as a quasi-coherent radiation source, but also a gas-detection scheme, which will be discussed.

The remainder of this paper will be organized into three sections. Section 2 will discuss the computational techniques used. Section 3 is broken into three subsections. In the first subsection, (3.A) of the results, we investigate the properties of a genetic-algorithm-optimized aperiodic design and compare them to a previously proposed resonant cavity design. A discussion of an emitter tuned to the Wien wavelength of a near-maximum operating temperature for the structure follows in the next subsection (3.B). Lastly, we discuss a

structure designed for an application as the emitting portion of a low-cost carbon monoxide (CO) detector (Subsection 3.C) and provide our conclusions in Section 4.

2. THEORY

We envision a structure composed of infinite slabs of material of varying aperiodic thicknesses as depicted in Fig. 1. Light is incident from air at an angle θ to the structure. Utilizing the transfer matrix method [18], we calculate the transmittance, reflectance, and absorbance of the structure for both TE and TM polarized light. We make use of experimental data for the wavelength-dependent indices of refraction, both real and imaginary parts, for silica, silicon, and tungsten [19] for the calculations done in this paper. Since the tungsten substrate is taken to be semi-infinite, the transmittance is identically zero, so that

$$A_{\mathrm{TE/TM}}(\lambda,\theta) = 1 - R_{\mathrm{TE/TM}}(\lambda,\theta), \tag{1}$$

where $A_{\mathrm{TE/TM}}$ is the TE/TM absorbance, $R_{\mathrm{TE/TM}}$ is the TE/TM reflectance, and λ is the wavelength. While we only calculate absorbance, reflectance, and, in principle, transmittance, we make use of Kirchhoff's second law and conservation of energy to equate absorbance ($A_{\mathrm{TE/TM}}$) and emittance ($\epsilon_{\mathrm{TE/TM}}$) under thermal equilibrium [20].

A. Fitness

We are interested in finding structures with highly directional and narrowband thermal emittance.

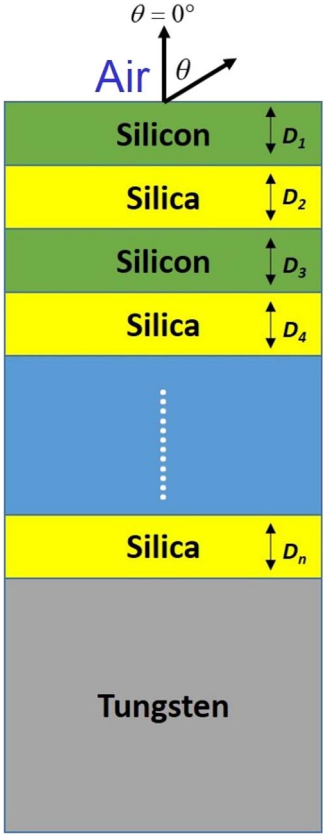

Fig. 1. Schematic of structure optimized by genetic algorithm coupled to the transfer matrix code. Incident light at an angle θ to the normal of the surface of the structure enters the n-layer alternating structure of silicon and silica above a semi-infinite tungsten substrate.

We used a genetic optimization algorithm to determine the best structure's dimensions for varying numbers of layers at a given wavelength, λ_0. The genetic algorithm is an iterative optimization procedure, which starts with a randomly selected population of potential solutions, and gradually evolves toward improved solutions, via the application of the genetic operators. These genetic operators are patterned after the natural selection process. In the initialization function, a population of chromosomes is created by random selection of values for the genes. The genetic algorithm then proceeds to iteratively generate a new population by the application of selection, crossover, and mutation operators.

More specifically, here we use the microgenetic algorithm. It has been shown that the microgenetic algorithm avoids premature convergence and shows faster convergence to the near-optimal region compared with the conventional large-population genetic algorithm for multidimensional problems [17,21,22]. The microgenetic algorithm starts with a small random population that evolves and converges after a few generations. At this point, keeping the best individual from the previously converged generation, a new random population is chosen, and the evolution process restarts.

We use tournament selection as the selection scheme in the genetic algorithm. In this method, a subpopulation of individuals is randomly chosen from the population and made to compete on the basis of their fitness values. The individual in the subpopulation with the highest fitness value wins the tournament, and is thus selected. The remaining members of the entire subpopulation are then put back into the general population, and the process is repeated. This selection scheme converges more rapidly and has a faster execution time compared to other competing schemes [23]. Once a pair of individuals is selected as parents, the basic crossover operator creates two offspring by combining the chromosomes of their parents. We use uniform crossover rather than single point crossover, as it has been found that microgenetic algorithm convergence is faster with uniform crossover [17,23]. An elitist strategy [24] is also employed, wherein the best individual from one generation is passed on to the next generation.

Specifically, we calculated the emittance of each structure as a function of angle for $0° \le \theta \le 90°$. We then minimized the fitness function, $F(\lambda_0)$,

$$F(\lambda_0) = \int_{0°}^{90°} \epsilon_{\mathrm{Total}}(\lambda_0,\theta)\mathrm{d}\theta, \tag{2}$$

subject to the constraint that $\epsilon_{\mathrm{Total}}(\lambda_0,\theta=0°) \ge 0.95$. Here, $\epsilon_{\mathrm{Total}}(\lambda_0,\theta) = [\epsilon_{\mathrm{TE}}(\lambda_0,\theta) + \epsilon_{\mathrm{TM}}(\lambda_0,\theta)]/2$. That is, we calculated the integral of the emittance over all angles θ at a given wavelength, λ_0, and minimized it subject to the constraint that the emittance at normal incidence was at least 95%. It is interesting to note that the fitness function that we use does not impose any constraints on the wavelength dependence of the emittance, since the structures are optimized at a single wavelength; however, simply by minimizing the integral of the emittance over all angles at a single wavelength [as seen in Fig. 2(a), for example], we also achieve narrowband emittance.

3. RESULTS

In this section, we discuss three genetic-algorithm-optimized structures for use as thermal emitters. The first structure is

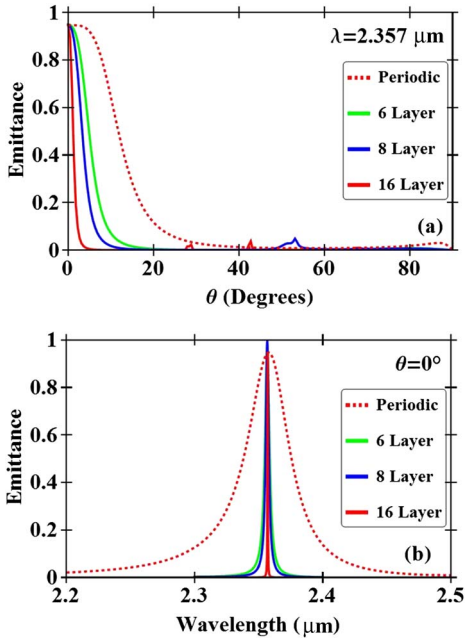

Fig. 2. (a) Emittance versus angle of an aperiodic multilayer structure of six, eight, and 16 alternating layers of silicon and silica over a semi-infinite tungsten substrate. The structure is optimized such that the integral of the emittance over all angles for $\lambda_0 = 2.357$ μm is minimized subject to the constraint that the emittance at normal incidence is greater than 0.95. The layer thicknesses of the optimized structure (in units of micrometers) are {1.53, 0.46, 0.17, 0.36, 2.32, 2.0} for the six-layer structure, {2.21, 0.45, 1.83, 1.92, 1.18, 1.49, 0.19, 2.07} for the eight-layer structure, and {2.25, 1.28, 0.49, 1.95, 2.27, 1.14, 0.85, 2.03, 0.33, 1.94, 2.34, 2.28, 0.92, 2.36, 1.27, 1.18} for the 16-layer structure. The red dashed line depicts a four-layer quarter-wave stack of alternating layers of silicon and silica followed by a half-wavelength resonant cavity over a semi-infinite tungsten substrate tuned to $\lambda_0 = 2.357$ μm. (b) Emittance versus wavelength of the same structures described in (a) at normal incidence.

optimized to operate at $\lambda_0 = 2.357$ μm for ease of comparison with a previously proposed resonant cavity design. The second structure is optimized to operate at the Wien wavelength corresponding to a near-maximum operating temperature for the materials used in the structure. Finally, the third structure discussed is optimized to operate at one of the molecular transition frequencies for CO for possible use in the emitting portion of an absorption spectroscopy detector.

A. Aperiodic Emitter

Using the transfer matrix method and genetic algorithm as outlined in Section 2, we investigated the properties of the aperiodic one-dimensional structures. We chose $\lambda_0 = 2.357$ μm as a first example in the infrared wavelength range.

For comparison, we define the angular full width at half-maximum (FWHM) $\delta\theta_n$ for the n-layer structure, calculating the width about $\theta = 0°$ for which the emittance is larger than half of the maximum achieved value as seen in Fig. 2(a). We also define the spectral FWHM $\delta\lambda_n$ for the n-layer structure, calculating the width about the wavelength at which we optimized the structure, λ_0, for which the emittance is larger than half of the maximum achieved value as seen in Fig. 2(b).

We consider structures of six, eight, and 16 layers composed of alternating layers of silicon and silica. In each case, we minimize the fitness function, $F(\lambda_0)$ [Eq. (2)], subject to the constraint that the normal incidence emittance $\epsilon_{\text{Total}}(\lambda_0, \theta = 0°) \geq 0.95$.

The optimized six-layer structure shows highly directional emittance with $\delta\theta_6 = 10.8°$ [Fig. 2(a)]. The optimized eight-layer structure improves upon this with $\delta\theta_8 = 7.2°$. The optimized 16-layer structure improves on the six-layer and eight-layer designs by nearly a factor of four and more than a factor of two, respectively, having $\delta\theta_{16} = 2.7°$. We also compare the genetically optimized structures with a previously proposed design consisting of a periodic quarter-wavelength stack with a half-wavelength resonant cavity over a semi-infinite tungsten substrate [7], which will heretofore be referred to as the periodic design, having $\delta\theta_{\text{Periodic}} = 26°$, an angular FWHM of more than twice that of the six-layer optimized structure [Fig. 2(a)].

Moving to the spectral FWHM, we note that the six-layer optimized structure has $\delta\lambda_6 = 8.8$ nm [Fig. 2(b)]. In comparison, the eight-layer optimized structure improves by more than a factor of two with $\delta\lambda_8 = 3.1$ nm. The 16-layer structure further improves this property by a factor of six over the eight-layer structure with a $\delta\lambda_{16} = 0.5$ nm. Compared to the genetic-algorithm-optimized aperiodic structures, the periodic structure exhibits much more broadband emittance, having $\delta\lambda_{\text{Periodic}} = 39.7$ nm [Fig. 2(b)]. These results can be found for at-a-glance comparison in Table 1.

In Fig. 3 we show the profile of the electric field amplitude, normalized with respect to the field amplitude of the incident plane wave for the six-layer genetic-algorithm-optimized aperiodic structure. The structure is excited by a normally incident plane wave at the resonant wavelength. We observe a large resonant enhancement of the electric field inside the silica layer adjacent to the tungsten substrate, which leads to greatly enhanced absorption in the substrate. Thus, one can

Table 1. Angular FWHM $\delta\theta_n$ and Spectral FWHM $\delta\lambda_n$ of the Structures Described in Fig. 2(a)

n	$\delta\theta_n$	$\delta\lambda_n$
6	10.8°	8.8 nm
8	7.2°	3.1 nm
16	2.7°	0.5 nm
Periodic	26°	39.7 nm

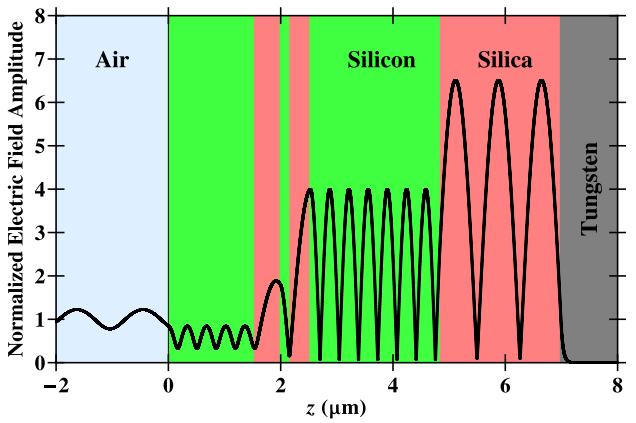

Fig. 3. Profile of the electric field amplitude, normalized with respect to the field amplitude of the incident plane wave for the six-layer genetic-algorithm-optimized aperiodic structure described in Fig. 2(a). The structure is excited by a normally incident plane wave at the resonant wavelength of $\lambda_0 = 2.357$ μm.

think of this structure as a silica cavity sandwiched between a tungsten substrate and a partially reflective aperiodic multilayer stack composed of alternating layers of silicon and silica. We also found that, when the wavelength or the angle of incidence is shifted away from resonance, the field enhancement rapidly decreases. This is consistent with the narrowband, highly directional emittance of the structure (Fig. 2).

Overall, the periodic structure exhibited both highly directional and narrowband emittance; however, even the six-layer genetic-algorithm-optimized aperiodic structure improved upon the directionality and increased the wavelength selectivity of the emittance, with the eight-layer and 16-layer structures further improving these features. As depicted in Fig. 2(a), it is important to note there is a trend of increasing angular selectivity as the number of layers increases. In addition, we found that there is a decrease in the outlying emittance in the $\theta > 60°$ range as the number of layers increases. In Fig. 2(b), a similar trend is seen: the wavelength selectivity of the emittance of the structure increases with the number of layers. Even the six-layer aperiodic structure shows vastly increased performance over the previously seen periodic design. The eight-layer aperiodic structure shows further increased performance, and the 16-layer aperiodic structure exhibits both extreme angular and spectral selectivity.

We then investigated the off-normal behavior of the emittance for both the genetic-algorithm-optimized aperiodic structures [Fig. 4(a)] as well as the periodic structure [Fig. 4(b)]. Similar trends were seen in the off-normal emittance bands as were seen with the normal. We looked specifically at the emittance at 30° and 60° and selected the peak wavelength emitted at those angles. There is a trend that as the angle θ increases, the peak of the emittance shifts to shorter wavelengths. This is due to the fact that the phase accumulation inside each layer decreases as the angle of incidence increases. This decrease can be compensated for by decreasing the wavelength [25]. This trend can also be seen in Fig. 5, where we

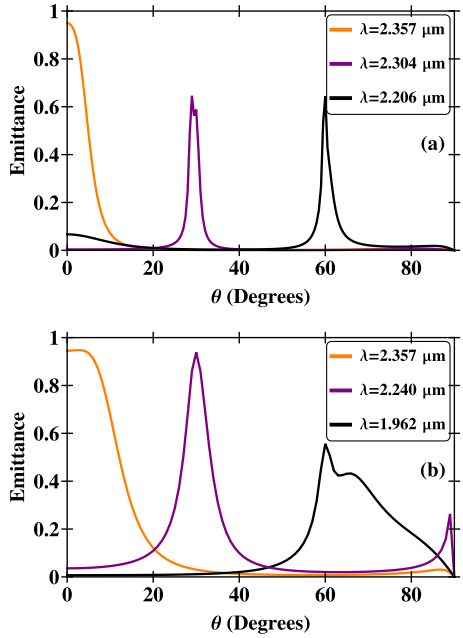

Fig. 4. (a) Angular emittance of the six-layer aperiodic structure described in Fig. 2(a). (b) Angular emittance for the periodic structure described in Fig. 2(a).

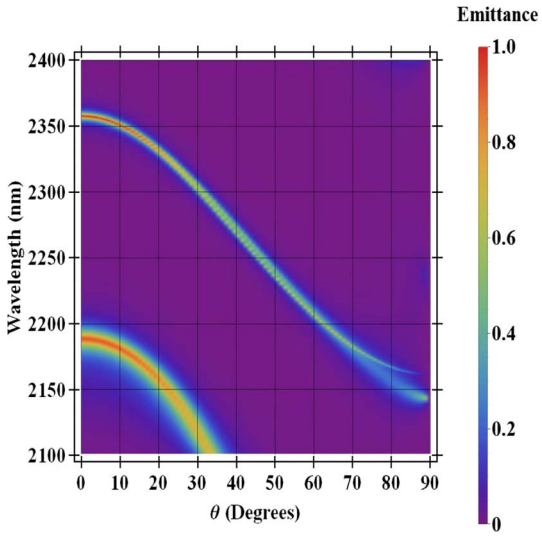

Fig. 5. Emittance as a function of wavelength and angle for the six-layer genetic-algorithm-optimized aperiodic structure described in Fig. 2(a).

show the emittance as a function of wavelength and angle for the six-layer genetic-algorithm-optimized aperiodic structure. Qualitatively, the periodic structure's peaks possess larger FWHM for both wavelength and angular emittance peaks than the genetic-algorithm-optimized aperiodic structures. We also note that the genetic-algorithm-optimized aperiodic structures' peaks shift more in angle with decreasing wavelength than do those of the resonant cavity design. This difference is related to the higher quality factor of the resonances, $Q = \lambda/\delta\lambda$, of the aperiodic structures, which leads to higher sensitivity to changes in angle of incidence.

B. Wien Wavelength

The Planck blackbody spectrum introduces temperature and wavelength dependence into the spectral radiance $B(\lambda, T)$ of a blackbody:

$$B(\lambda, T) = \frac{2hc^2}{\lambda^5}\frac{1}{e^{\frac{hc}{\lambda k_B T}-1}}, \tag{3}$$

where h is Planck's constant, c is the speed of light, and k_B is the Stefan–Boltzman constant. In principle, the power spectrum $\mu(\lambda)$ for any material or structure with emittance $\epsilon(\lambda)$ is

$$\mu(\lambda) = \epsilon(\lambda)B(\lambda, T). \tag{4}$$

Here, we seek to maximize such emittance while accounting for the melting points of the materials used. We can calculate the maximum of B as a function of wavelength by setting $\partial B/\partial\lambda = 0$. This results in the following equation:

$$\frac{xe^x}{e^x - 1} = 5, \tag{5}$$

where $x = hc/\lambda k_B T$. Once solved, Wien's displacement law is extracted:

$$\lambda_{\max} = \frac{hc}{xk_B T}, \tag{6}$$

where x is the solution of Eq. (5), $x = 4.96511\ldots$.

Considering melting points for silicon, silica, and tungsten, silicon has the lowest melting point of 1690 K. Allowing a small safety margin, we reduce this temperature to 1500 K and make use of Wien's displacement law to calculate the

appropriate wavelength for maximum power output to be $\lambda = 1.931$ μm. As before, we consider structures of six, eight, and 16 layers composed of alternating layers of silicon and silica. In each case, we minimize the fitness function, $F(\lambda_0)$ [Eq. (2)], subject to the constraint that the normal incidence emittance $\epsilon_{\text{Total}}(\lambda_0, \theta = 0°) \geq 0.95$.

We chose this wavelength and optimized the same six-, eight-, and 16-layer aperiodic structures for angular and wavelength-selective emittance here. Again, as we saw in Fig. 2, the same trends appear in Fig. 6, with the six-layer structure showing a well-defined peak in both angular and wavelength space, the eight-layer structure improving upon what the six-layer offered, and the 16-layer further increasing angular and wavelength selectivity. More concretely, the six-layer structure offers a selective emitter, with a $\delta\theta_6 = 14.4°$ and $\delta\lambda_6 = 11.1$ nm. The eight-layer optimized structure performs better by nearly a factor of two with a $\delta\theta_8 = 8.1°$ and $\delta\lambda_8 = 3.2$ nm. The 16-layer optimized structure outperforms the eight-layer structure by another factor of two and is a full factor of four better than the six-layer structure with a $\delta\theta_{16} = 3.6°$ and $\delta\lambda_{16} = 0.5$ nm. These results can be found for at-a-glance comparison in Table 2.

C. Aperiodic Structure as the Emitting Portion of a Detector

CO is a colorless, odorless, and tasteless gas that is poisonous to humans. One of the molecular resonances of CO occurs at $\lambda = 4.7$ μm [26]. Here, we consider constructing the emitting portion of a low-cost detector for CO utilizing a quasi-coherent thermal source emitting at the transition frequency.

Table 2. Angular FWHM $\delta\theta_n$ and Spectral FWHM $\delta\lambda_n$ of the Structures Described in Fig. 6(a)

n	$\delta\theta_n$	$\delta\lambda_n$
6	14.4°	11.1 nm
8	8.1°	3.2 nm
16	3.6°	0.5 nm

By heating the designed structure, light is emitted at one of the resonant frequencies of CO. Via absorption spectroscopy, one may use a detector that searches for dips in the intensity of the 4.7 μm light, which would signify an increase of the concentration of CO in the air, thereby setting off the alarm.

With this application in mind, we chose $\lambda_0 = 4.7$ μm, and we designed optimized structures. These results are depicted in Fig. 7. Again, the same trends are found that increasing the number of layers increases both the angular and wavelength selectivity. At 4.7 μm, the selectivity of each of the six-, eight-, and 16-layer structures was notably higher than at previously optimized wavelengths.

At this wavelength, the six-layer structure performed a factor of two better than the structure optimized for $\lambda_0 = 1.931$ μm with a $\delta\theta_6 = 8.2°$ and $\delta\lambda_6 = 4.4$ nm. The eight-layer structure showed marginal improvement over the six-layer with $\delta\theta_8 = 5.4°$ and $\delta\lambda_8 = 2.2$ nm; however, the 16-layer optimized structure showed more than a factor of three overall improvement, with a $\delta\theta_{16} = 1.8°$ and $\delta\lambda_{16} = 0.2$ nm. These results can be found for at-a-glance comparison in Table 3.

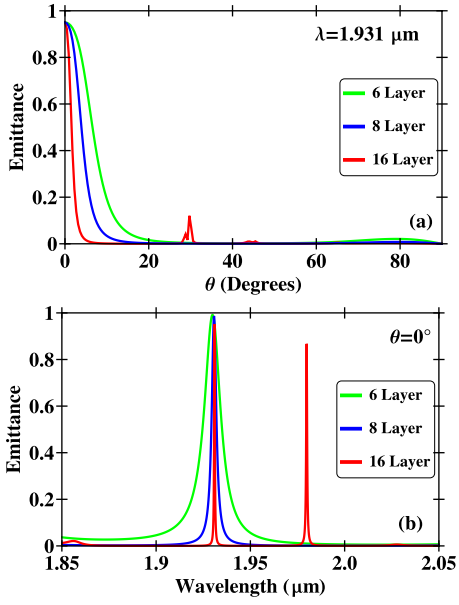

Fig. 6. (a) Emittance versus angle of an aperiodic multilayer structure of six, eight, and 16 alternating layers of silicon and silica over a semi-infinite tungsten substrate. The structure is optimized such that the integral of the emittance for $\lambda_0 = 1.931$ μm over all angles is minimized subject to the constraint that the emittance at normal incidence is greater than 0.95. The layer thicknesses of the optimized structure (in units of micrometers) are {1.81, 0.36, 0.12, 1.83, 0.43, 1.09} for the six-layer structure, {1.81, 0.29, 0.72, 0.35, 0.72, 1.82, 0.72, 0.26} for the eight-layer structure, and {1.55, 0.9, 1.56, 1.63, 1.21, 1.62, 0.39, 1.24, 1.30, 0.34, 0.77, 1.87, 1.54, 0.23, 0.24, 0.24} for the 16-layer structure. (b) Emittance versus wavelength of the same aperiodic structures described in (a) at normal incidence.

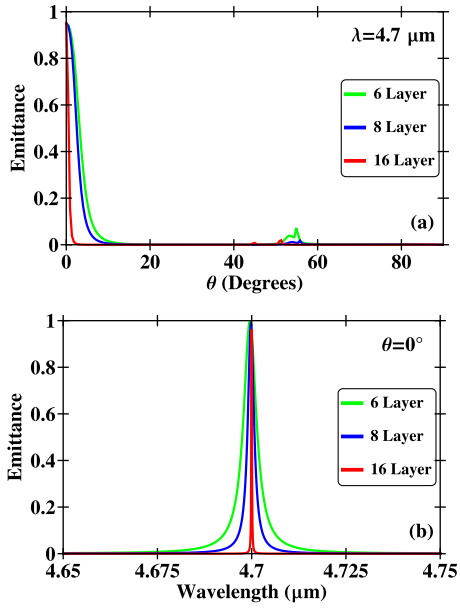

Fig. 7. (a) Emittance versus angle of an aperiodic multilayer structure of six, eight, and 16 alternating layers of silicon and silica over a semi-infinite tungsten substrate. The structure is optimized such that the integral of the emittance for $\lambda = 4.7$ μm over all angles is minimized subject to the constraint that the emittance at normal incidence is greater than 0.95. The layer thicknesses of the optimized structure (in units of micrometers) are {3.77, 0.9, 3.76, 4.49, 4.62, 3.16} for the six-layer structure, {3.75, 0.91, 2.40, 4.53, 4.51, 1.28, 3.93, 2.94} for the eight-layer structure, and {4.47, 0.88, 0.39, 1.02, 0.35, 0.91, 1.14, 4.00, 2.03, 2.39, 1.72, 3.38, 0.34, 0.99, 3.04, 4.15} for the 16-layer structure. (b) Emittance versus wavelength of the same aperiodic structures described in (a) at normal incidence.

Table 3. Angular FWHM $\delta\theta_n$ and Spectral FWHM $\delta\lambda_n$ of the Structures Described in Fig. 7(a)

n	$\delta\theta_n$	$\delta\lambda_n$
6	8.2°	4.4 nm
8	5.4°	2.2 nm
16	1.8°	0.2 nm

4. CONCLUSIONS

We have designed a series of aperiodic structures that have been optimized to produce narrow angular emittance profiles and also display narrow-wavelength emittance. We compared the angular and spectral FWHMs of the genetic-algorithm-optimized aperiodic structures to the ones of the resonant cavity design. We have demonstrated that angular selectivity increases with the number of layers and noticed a strong correlation between angular selectivity and spectral selectivity. We have presented an additional structure that has a use as a quasi-coherent emitter optimized to operate at the Wien wavelength corresponding to a near-maximum operating temperature for a silica–silicon structure. Finally, we have outlined a low-cost method for constructing the emitting portion of an absorption spectroscopy detector for CO.

As final remarks, we have discussed several specific structures that can be tuned to emit at a wide variety of wavelengths. We note that due to the wavelength dependence of the dielectric permittivity of the materials used in the design, one cannot simply scale the layer thicknesses by a factor to scale the operating wavelength by that same factor. In other words, the optimized designs are not scale invariant, so the optimization process must be carried out at the new desired wavelength. In all cases, we found that the optimal structures were unique. In other words, if the stochastic genetic optimization process is repeated, it converges to the same result. Finally, for structures designed as emitters, there is a question of how performance will change as temperature is varied. It is known that temperature variations tend to primarily modify the material losses [27]. We found that, if the material losses change, we can still use the same genetic-algorithm-optimization approach to design highly directional, narrowband emitters. Thus, our approach can be used to design structures at a desired operating temperature. We also found that the effect of layer thickness variations due to thermal expansion on emittance can be neglected [27].

ACKNOWLEDGMENTS

This research was supported by the National Science Foundation (Award Nos. 1102301, 1263236, and 0968895), and a Fund for Innovation in Engineering Research (FIER) grant from the Louisiana State University College of Engineering. Jonathan P. Dowling also acknowledges support from the Air Force Office of Scientific Research and the Army Research Office.

REFERENCES

1. M. Ghebrebrhan, P. Bermel, Y. X. Yeng, I. Celanovic, M. Soljačić, and J. D. Joannopoulos, "Tailoring thermal emission via Q matching of photonic crystal resonances," Phys. Rev. A **83**, 033810 (2011).
2. E. Rephaeli and S. Fan, "Absorber and emitter for solar thermo-photovoltaic systems to achieve efficiency exceeding the Shockley-Queisser limit," Opt. Express **17**, 15145–15159 (2009).
3. J. J. Greffet, R. Carminati, K. Joulain, J. P. Mulet, S. Mainguy, and Y. Chen, "Resonant transmission through a metallic film due to coupled modes," Nature (London) **416**, 61–64 (2002).
4. D. Chan, M. Soljačić, and J. D. Joannopoulos, "Thermal emission and design in 2D-periodic metallic photonic crystal slabs," Opt. Express **14**, 8785–8796 (2006).
5. J. G. Fleming, S. Y. Lin, I. El-Kady, R. Biswas, and K. M. Ho, "All-metallic three-dimensional photonic crystals with a large infrared bandgap," Nature **417**, 52–55 (2002).
6. M. Florescu, H. Lee, I. Puscasu, M. Pralle, L. Florescu, D. Ting, and J. P. Dowling, "Improving solar cell efficiency using photonic band-gap materials," Sol. Energy Mater. Sol. Cells **91**, 1599–1610 (2007).
7. I. Celanovic, D. Perreault, and J. Kassakian, "Resonant-cavity enhanced thermal emission," Phys. Rev. B **72**, 075127 (2005).
8. D. L. C. Chan, M. Soljačić, and J. D. Joannopoulos, "Thermal emission and design in one-dimensional periodic metallic photonic crystal slabs," Phys. Rev. E **74**, 016609 (2006).
9. C. Arnold, F. Marquier, M. Garin, F. Pardo, S. Collin, N. Bardou, J. L. Pelouard, and J. J. Greffet, "Coherent thermal infrared emission by two-dimensional silicon carbide gratings," Phys. Rev. B **86**, 035316 (2012).
10. M. Laroche, C. Arnold, F. Marquier, R. Carminati, J. Greffet, S. Collin, N. Bardou, and J. Pelouard, "Highly directional radiation generated by a tungsten thermal source," Opt. Lett. **30**, 2623–2625 (2005).
11. S. Han and D. Norris, "Beaming thermal emission from hot metallic bull's eyes," Opt. Express **18**, 4829–4837 (2010).
12. G. Biener, N. Dahan, A. Niv, V. Kleiner, and E. Hasman, "Highly coherent theremal emission obtained by plasmonic bandgap structures," Appl. Phys. Lett. **92**, 081913 (2008).
13. N. Mattiucci, G. D'Aguanno, A. Alú, C. Argryopoulos, J. Foreman, and M. J. Bloemer, "Taming the thermal emissivity of metals: a metamaterial approach," Appl. Phys. Lett. **100**, 201109 (2012).
14. E. J. Reed, M. Soljačić, and J. D. Joannopoulos, "Maxwell equation simulations of coherent optical photon emission from shock waves in crystals," Phys. Rev. E **75**, 056611 (2007).
15. E. J. Reed, M. Soljačić, R. Gee, and J. D. Joannopoulos, "Molecular dynamics simulations of coherent optical photon emission from shock waves in crystals," Phys. Rev. B **75**, 174302 (2007).
16. G. Liang, P. Han, and H. Wang, "Narrow frequency and sharp angular defect mode in one-dimensional photonic crystals from a photonic heterostructure," Opt. Lett. **29**, 192–194 (2004).
17. K. Krishnakumar, "Micro-genetic algorithms for stationary and non-stationary function optimization," Proc. SPIE **1196**, 289 (1989).
18. C. M. Cornelius and J. P. Dowling, "Modification of Planck blackbody radiation by photonic band-gap structures," Phys. Rev. A **59**, 4736–4746 (1999).
19. D. R. Lide, *CRC Handbook of Chemistry and Physics*, 88th ed. (CRC Press, 2007).
20. E. U. Condon, *Fundamentals of Statistical and Thermal Physics* (McGraw-Hill, 1965).
21. D. E. Goldberg and K. Deb, "A comparative analysis of selection schemes used in genetic algorithms," in *Foundations of Genetic Algorithms*, G. J. E. Rawlins, ed. (Morgan Kaufmann, 1997), pp. 69–93.
22. K. Deb and S. Agrawal, "Understanding interactions among genetic algorithm parameters," in *Foundations of Genetic Algorithms*, W. Banzhaf and C. Reeves, eds. (Morgan Kaufmann, 1999), pp. 268–269.
23. D. E. Goldberg, K. Deb, and J. H. Clark, "Genetic algorithms, noise, and the sizing of populations," Comp. Syst. **6**, 333–362 (1991).
24. J. M. Johnson and Y. Rahmat-Samii, "Genetic algorithms in electromagnetics," in *Proceedings of the IEEE International Symposium on Antennas and Propagation* (IEEE, 1996), pp. 1480–1483.
25. N. Tessler, S. Burns, H. Becker, and R. H. Friend, "Suppressed angular color dispersion in planar microcavities," Appl. Phys. Lett. **70**, 556–558 (1997).
26. A. L. Smith, *The Coblentz Society Desk Book of Infrared Spectra* (The Coblentz Society, 1982).
27. Y. X. Yeng, M. Ghebrebrhan, P. Bermel, W. R. Chan, J. D. Joannopoulos, M. Soljačić, and I. Celanovic, "Enabling high-temperature nanophotonics for energy applications," Proc. Natl. Acad. Sci. USA **109**, 2280–2285 (2012).